

# PADME: A Deep Learning-based Framework for Drug-Target Interaction Prediction

Authors: Qingyuan Feng, Evgenia Dueva, Artem Cherkasov and Martin Ester\*

\*ester@sfu.ca

## Abstract

*In silico* Drug-target Interaction (DTI) prediction is an important and challenging problem in medicinal chemistry with a huge potential benefit to the pharmaceutical industry and patients. Most existing methods for DTI prediction generally have binary endpoints, which could be an oversimplification of the problem. With the advent of deep learning, some deep learning models were devised to solve the DTI prediction problem, but most of them still use binary endpoints, and they are generally unable to handle cold-target problems, i.e., problems involving target protein that never appeared in the training set. We contrived PADME (Protein And Drug Molecule interaction prEdiction), a framework based on Deep Neural Networks, to predict real-valued interaction strength between compounds and proteins. PADME inputs both compound and protein information into the model, so it is applicable to cold-target problems. To our knowledge, we are also the first to incorporate Molecular Graph Convolution (MGC) into the model for compound featurization. We used different Cross-Validation split schemes and different metrics to measure the performance of PADME on multiple datasets (in which we are the first to use ToxCast for such problems), and PADME consistently dominates baseline methods. We also conducted a case study, predicting the interaction between compounds and androgen receptor (AR) and compared the prediction results with growth inhibition activity of the compounds in NCI60, which also gave us satisfactory results, suggesting PADME's potential in drug development. We expect different variants of PADME to be proposed and experimented on in the future, and we believe Deep Learning will transform the field of cheminformatics.

## Introduction

Finding out the binding activities between compounds (candidate drugs) and target proteins is of crucial importance in the drug development process. However, it is extremely expensive and time-consuming to be done in wet lab experiments, while virtual screening using computational (also called "*in silico*") methods to predict the interactions between compounds and target proteins could greatly accelerate the drug development process at a significantly reduced cost. Machine learning models for drug-target interaction (DTI) prediction are often used in *in silico* drug design (Ding et al., 2014).

Datasets often used for training and evaluating machine learning models for DTI prediction include enzymes, ion channels, nuclear receptors, etc. (Yamanishi et al., 2008) They contain binary labels for the interaction of certain drug-target pairs, with 1 indicating a known interaction. Recently, the community has also explored the usage of datasets with real-valued interaction strength measurements (Pahikkala et al., 2014; He et al., 2017), which include Davis dataset (Davis et al., 2011) that uses inhibition constant ( $K_i$ ), Metz dataset (Metz et al., 2011) that uses dissociation constant ( $K_d$ ) and KIBA dataset (Tang et al., 2014).

Existing traditional machine learning methods for predicting DTI can be roughly divided into similarity-based and feature-based approaches. Similarity-based methods depend on the assumption that

compounds with similar structures should have similar effects. Feature-based methods construct feature vectors as input, which are generated by combining descriptors of compounds with descriptors of targets, and the feature vectors serve as inputs of algorithms like SVM (He et al., 2016).

SimBoost (He et al., 2017) and KronRLS (Pahikkala et al., 2014) are two state-of-the-art methods for DTI prediction. KronRLS is based on Regularized Least Squares and utilizes the similarity matrices for drugs and targets to get the parameter values. SimBoost is a feature-based method, but in its feature construction, similarity matrices of the drugs and targets are also involved. These methods can both predict continuous values and binarized values. However, these methods either rely on simple similarities, or require a lot of human knowledge to define the relevant features of proteins and compounds, unable to model highly complex interactions within compound molecules (Mayr et al., 2016) and between the compounds and target proteins. Deep neural networks promise to address these challenges as discussed below.

Deep learning has been enjoying an ever-rising popularity in the past few years. As a highly successful field of machine learning, deep learning methods have seen wide and exciting applications in computer vision, speech recognition, natural language processing, reinforcement learning, and drug-target interaction prediction. Deep learning can automatically extract important features from the input data, synthesize and integrate low-level features into high-level features, and capture complicated nonlinear relationships in a dataset (LeCun et al., 2015; Schmidhuber, 2015). Deep learning-based DTI prediction has been shown to consistently outperform the existing methods and has become the new “golden standard” (Dahl et al., 2014; Unterthiner et al., 2014; Ma et al., 2015).

The current deep learning approaches to drug-target interaction prediction can be roughly categorized based on their neural network types and prediction endpoints. Simple feedforward neural networks (including Deep Belief Networks, or DBN), Convolutional Neural Networks (CNN) and Recurrent Neural Networks (RNN) have been used, among which feed-forward networks and CNN are more popular, possibly due to their simplicity (Xu and Pei, 2017). To our knowledge, all existing deep learning methods, except those that have 3D structural information as input, treat the problem as a classification problem, most of which are binary, namely active/inactive. Though there are deep learning models using 3D structural information that yield good results (Wallach et al., 2015; Gomes et al., 2017), the requirement of 3D structural information limits the applicability of a model since such information is not always available, so we do not consider them in this paper. As deep learning for drug-target interaction is still in its infancy, the current models have much room for improvement, as discussed in the following.

**First**, formulating the problem as a classification problem has several disadvantages: obviously, the classification result depends on a predefined binarization threshold, which introduces some arbitrariness into the data; some useful information is lost, for instance, true-negative and missing values may not be discriminated (Pahikkala et al., 2014; He et al., 2017); on the other hand, if we formulate it as a regression problem, not only can we avoid the problems above, but given the regression results, the real-valued outputs can be easily converted to a ranking or to a binary classification. Some existing methods that do not make use of deep neural networks formulate the problem as a regression problem, in which the interaction strength between the drug molecule and the target protein is a real number, serving as the regression target (He et al., 2017). Common real-valued interaction strength metrics include inhibition constant ( $K_i$ ), dissociation constant ( $K_d$ ), 50% inhibition concentration ( $IC_{50}$ ), etc.

**The second problem** is that most of the existing deep-learning methods do not incorporate the target protein information into the network, except very few recent works, like (Wen et al., 2017). As a result, the models are unable to solve the “cold target” problem, i.e. to predict the drug-target interactions for new target proteins.

DeepDTI (Wen et al., 2017) addressed the second problem by incorporating the protein information with the compound vector. It uses the classical Extended-Connectivity Fingerprint (ECFP) (Rogers and Hahn, 2010) for describing compounds, which relies on a fixed hashing function and cannot adjust to specific problems at hand, leaving some room for improvement. DeepDTI concatenates ECFP and Protein Sequence Composition (PSC) descriptors (Cao et al., 2013) (for describing target proteins’ sequence information) to construct a feature vector, which is fed into a Deep Belief Network (DBN) to predict a binary endpoint. DeepDTI outperformed the state-of-the-art methods on a dataset extracted from DrugBank.

In this paper, we propose PADME (Protein And Drug Molecule interaction prEdiction), a deep-learning based framework for predicting DTI. We tackle the limitations of the existing methods, with a real-valued interaction strength as the prediction endpoint instead of classification results, and, to address the cold-start problem (drugs or targets that are absent from the training set exist in the test set), PADME utilizes a combination of drug and target features/fingerprints as the input vector, similar to (Wen et al., 2017), but unlike the DBN they used, we use simple feedforward network to connect the input vector to the output layer. We adopted Molecular Graph Convolution (MGC) to learn the feature vectors of the candidate drug molecules, which is more flexible than the existing methods, able to adapt the mapping function by updating the weights in the neural network based on the task at hand (Kearnes et al., 2016; Tran et al., 2017). We are the first to integrate MGC with protein descriptors for the DTI problem. Compared to the state-of-the-art methods based on similarity matrices for DTI regression task including SimBoost (He et al., 2017) and KronRLS (Pahikkala et al., 2014), our model is much more scalable, since it does not require computing drug-drug and target-target similarity matrices or factorizing interaction matrices, which could become a daunting task for a large number of drugs or targets. In addition to the datasets used by previous researches, we also propose using the ToxCast dataset, and we believe this large high-quality dataset, with its much larger variety of proteins, could be another “gold standard” benchmarking dataset for future researches.

We conducted computational experiments with different cross validation settings and used different metrics. The results demonstrated the dominance of PADME over baseline methods across all experimental settings.

PADME supports the drug discovery and design process for given protein targets (target-based prediction). PADME can also provide interesting insights to researchers for studying the strongly binding target proteins to specific potent drug compounds (compound-based prediction), which could potentially help advance researches in the field, like identifying novel molecular pathways important in cancer cells. We used the US National Cancer Institute human tumour cell line anticancer drug screen data (NCI60), a dataset recording the *in vitro* drug response of cancer cell lines (Shoemaker, 2006), to find the effectiveness of compounds in suppressing cancer cells’ growth. In a case study, we selected the androgen receptor (AR), which is known to be of crucial importance in prostate cancer development (Yap et al., 2016). We applied PADME to predict the interaction strength between compounds and AR, then

evaluated the list of predictions using the compounds' cell growth inhibition activities in prostate cancer cell lines. The results suggested that the predictions of PADME have practical implications.

The subsequent sections of the paper are organized as follows. Section 2 will introduce the methodology of PADME, including methods for compound featurization, protein featurization, and network structure. Section 3 will present the experiments conducted, introducing the baseline methods, datasets used, experimental design, and the experimental results. Section 4 is a discussion, which involves some clarifications of the implementation and design choices, and also pointing the readers to the possible future directions to further this work. Section 5 concludes the whole paper.

## Methodology

We introduce PADME as a deep learning-based DTI prediction model which combines the compound (candidate drug) molecule and target protein feature vectors. We consider two alternative versions of PADME, one that uses MGC as the compound featurization method and one that uses ECFP (Rogers and Hahn, 2010) as the compound featurization method. For the protein descriptor we use the PSC, which records the amino acid, dipeptide and tripeptide composition of the target protein (Cao et al., 2013). Note that PADME is in fact compatible with all kinds of protein descriptors and molecular featurization methods. The compound vector (ECFP or generated through MGC in our study) is concatenated with a target protein vector to form the Combined Input Vector (CIV) for the neural network. PADME predicts a real-valued interaction strength, i.e., it solves a DTI regression problem. The structure of the network is shown in Figure 1: if we use the molecular graph convolutional network to get the molecular vector, that network will be trained together with the feedforward network connecting the CIV to the prediction endpoint, i.e., in an end-to-end fashion. MGC (Kearnes et al., 2016; Tran et al., 2017) is a type of Convolutional Neural Network which learns a latent vector representing the compound from the its graphical representation. It is more complicated yet more flexible than ECFP. More details are presented later in this section.

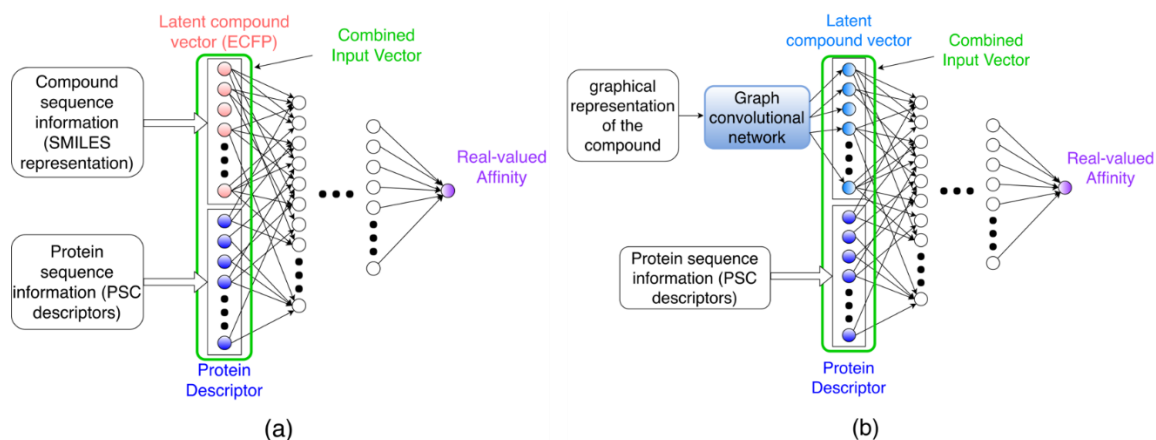


Figure 1. a) PADME-ECFP illustration. The Extended-Connectivity Fingerprint was used as the molecular input to the model. b) PADME-GraphConv illustration. Note that the graph convolutional network generating the latent molecular vector is trained together with the rest of the network, while the protein descriptor generation process is independent from the training of the network. The black dots represent omitted neurons and layers.

## 1. Compound featurization

There has been a lot of work focusing on representing small molecules (compounds) for computer programs. Among the traditional molecular descriptors and fingerprints, ECFP, invented by (Rogers and Hahn, 2010), is widely adopted as the state-of-the-art method for compound featurization (Duvenaud et al., 2015), and was also used in (Wen et al., 2017). However, it has a fixed set of mapping and hashing functions, unable to be tailored for the specific task at hand.

To our knowledge, the work by (Duvenaud et al., 2015) was the first to learn a “neural fingerprint” (compound feature vector) using graph convolution, outperforming the ECFP baseline and offering some good interpretability. Later, (Tran et al., 2017) proposed another graph convolution model which had good performance. Following the convention in (Wu et al., 2017) and their Deepchem package, we call this model GraphConv, which stands for “graph convolution”. It is similar in idea to (Duvenaud et al., 2015), except a few differences, like the use of batch normalization layers, and doing the sum of atom feature vectors after all convolutional layers.

They are just some examples of the recent works using deep neural networks to generate compound feature vectors (Kearnes et al., 2016). Unlike the traditional fingerprints like ECFP which only depend on the molecule, compound feature vectors generated using deep neural networks depend on both the molecule and the prediction task (Boolean or continuous). To generate the feature vector, these methods construct graph convolutional neural networks, which are trained together with the rest of the network used for prediction. In the graphical representation, the atoms are denoted by nodes, while the bonds are denoted by edges. The MGC takes into account the neighbors of a node when computing the intermediate feature vector for a specific node, and the same operation is applied to the neighborhood of each node (atom), hence it is similar in idea to ordinary convolutional networks typically used in Computer Vision (Goodfellow et al., 2016).

Due to the GraphConv model being more recent and its source code more readily available, we use the GraphConv model as a representative of the MGC models under the time and resource constraints.

We applied both types of compound featurization methods: ECFP and GraphConv, then compared their performances against each other.

## 2. Target Protein featurization

Mapping a protein into a representative feature vector is a task in proteochemometrics. However, most existing methods in proteochemometrics require lots of human expert knowledge to curate and compose the protein feature vector, and often involves some 3D structural information (Westen et al., 2011; Qiu et al., 2016), so we deem them as undesirable. As protein 3D structural information is often not available, we only consider sequence information in this work to make our model more generally applicable, though at the cost of reduced interpretability.

Nonetheless, there still exist many schemes to represent the target protein as a feature vector based on its amino acid sequence information.

(Wen et al., 2017) used Protein Sequence Composition (PSC) Descriptor, which has 8420 entries for each protein, consisting of amino acid composition (AAC), dipeptide composition (DC), and tripeptide composition (TC) (Cao et al., 2013). It seems to capture very rich information and does not transform the

protein as much as some other protein descriptors (which implies fewer human knowledge required and less information loss), which we think could be a desirable attribute as the input to a neural network. In addition to the 8420 entries for each protein sequence, we added an additional binary entry signaling the phosphorylation status so that the Davis dataset (see below) can be presented more accurately, with ‘1’ denoting phosphorylated and ‘0’ otherwise, so there are 8421 entries in total.

(Mousavian et al., 2016) used PSSM (Position Specific Scoring Matrix) descriptor to represent the protein, which focuses on dipeptide sequences and is related to the evolutionary history of proteins (Sharma et al., 2013). It is observed that PSSM yielded some pretty good performance. Other popular protein sequence descriptors include Autocorrelation, CTD (Composition, Transition and Distribution) descriptor, Quasi-sequence order, etc (Cao et al., 2013).

As PSC contains rich information (like tri-peptide sequence occurrence) with high dimensionality, and that PSC has already shown promising performance in deep-learning based models for DTI prediction (Wen et al., 2017), we use PSC in this research due to the time and resource constraints. There could be future comparison studies of the performance of PSC and other protein featurization methods as an extension to this work.

### 3. Network structure

Unlike the (Wen et al., 2017) paper which uses deep belief network, we used simple feedforward neural network (FNN) taking the Combined Input Vector (CIV) as the input, because deep belief network has fallen out of favor in the deep learning community after regularization techniques like batch normalization were introduced to improve the performance of FNNs. There could be a single output neuron, called single-task network, or multiple output neurons, which is called multi-task network. Although we only consider regression problems in this paper, PADME can also be used for constructing classification models with minimal changes, by either binarizing the continuous prediction results or directly using a softmax layer as the output layer.

For Regularization, we used Early Stopping, Dropout and Batch Normalization techniques. Hyperparameters like dropout rates are being automatically searched to find the best set of them to run cross-validation, which are elaborated in the “Experimental Design” section. The Adam optimizer was used to train the network. The activation functions used for fully connected layers are all Rectified Linear Units (ReLU).

## Experiments

### 1. Baseline methods

There are two baseline methods used as comparisons: SimBoost (He et al., 2017) and KronRLS (Pahikkala et al., 2014), which are state-of-the-art methods for the DTI regression task.

SimBoost

Simboost predicts continuous DTI value using gradient boosting regression trees. Each drug-target pair corresponds to a continuous DTI value, and the authors defined 3 types of features to characterize the drug-target pairs: type 1 features for individual entities (drugs or targets); type 2 features, derived from the drug and target similarity networks, include values like Eigenvector Centrality and PageRank score; type 3 features, which are derived from drug-target interaction network. The 3 types of features are concatenated to form a feature vector for each drug-target pair.

Let  $x_i \in R^d$  denote the vector of features for the  $i$ -th drug-target pair, while  $y_i \in R$  is its binding affinity. The score  $\hat{y}_i$  predicted for input  $x_i$  is computed as follows:

$$\hat{y}_i = \phi(x_i) = \sum_{k=1}^K f_k(x_i), f_k \in F$$

Where  $K$  is the number of regression trees and  $F$  is the space of possible trees. To learn the set of trees  $f_k$ , they defined a regularized objective function:

$$L(\phi) = \sum_i l(\hat{y}_i, y_i) + \sum_k \Omega(f_k)$$

Where  $l$  is a loss function that evaluates the prediction error, while  $\Omega$  is a function that penalizes overfitting. The model is trained additively: for each iteration  $t$ ,  $F$  is searched to find a new tree  $f_t$  that optimizes the objective function, which is added to the ensemble afterwards. Trees that optimize  $L^{(t)}$  are iteratively added to the model for a number of pre-specified iterations.

$$\begin{aligned} L^{(t)} &= \sum_{i=1}^n l(y_i, \hat{y}_i^{(t)}) + \sum_{i=1}^t \Omega(f_i) \\ &= \sum_{i=1}^n l(y_i, \hat{y}_i^{(t-1)} + f_t(x_i)) + \sum_{i=1}^t \Omega(f_i) \end{aligned}$$

SimBoost cannot handle the cold-start problem, which means it does not work for pairs in the test set with a drug or target that is absent from the training set.

## KronRLS

KronRLS stands for Kronecker Regularized Least Squares. It learns a prediction function  $f(x)$  for drug-target pairs, with the following objective function (definition of  $x$  and  $y$  are similar to SimBoost):

$$J(f) = \sum_{i=1}^m (y_i - f(x_i))^2 + \lambda \|f\|_k^2$$

Where  $\|f\|_k^2$  is the norm of  $f$ . A minimizer of the objective function is:

$$f(x) = \sum_{i=1}^m a_i k(x, x_i)$$

In which  $k$  is a kernel function, which can be a similarity measure between two drug-target pairs. Given the similarity matrices  $K_d$  and  $K_t$  for drugs and targets, respectively, the similarity matrix  $K$  for drug-target pairs can be computed by  $K_d \otimes K_t$ , in which  $\otimes$  denotes Kronecker product. If the training set contains all possible drug-target pairs, the parameter vector  $a$  can be obtained by solving the system of linear equations:

$$(K + \lambda I)a = y$$

Where  $I$  is an identity matrix whose number of rows equals the number of all possible drug-target pairs. It could be solved by Kronecker algebraic optimization. If the training set does not contain all drug-target pairs, the authors suggested using conjugate gradient combined with Kronecker algebraic optimization to get the parameters  $a$ .

## 2. Datasets and tools

We use the datasets as used in (He et al., 2017), which are some kinase inhibitor datasets. Following its naming convention, we call them Davis dataset (Davis et al., 2011), Metz dataset (Metz et al., 2011) and KIBA dataset (Tang et al., 2014), respectively. However, the versions of these datasets curated by (Pahikkala et al., 2014) that (He et al., 2017) used was slightly different from the original dataset, and (Pahikkala et al., 2014) did not give the corresponding justifications. We thus used the data prepared by the respective original authors, then preprocessed them ourselves. We assume the observations within each dataset are under the same experimental settings. Metz dataset contained some imprecise values, which we discarded in the preprocessing step.

Because of the limitations of SimBoost and KronRLS, we filtered the aforementioned datasets. The original KIBA dataset contains 52498 compounds, a large proportion of which only have the interaction values with very few proteins. Considering the huge compound similarity matrix required and the time-consuming matrix factorization used in SimBoost, it would be infeasible to work directly on the original KIBA dataset. Thus, we had to filter it rather aggressively so that the size becomes more manageable. This suggests that PADME, which does not require drug-drug or target-target similarity matrices or matrix factorization, is much more scalable than KronRLS and SimBoost, both of which have at least  $O(n^2)$  time and space complexity. We chose to use a threshold of 6 (drugs and targets with no more than 6 observations are removed), looser than the threshold of 10 used in (He et al., 2017), hoping that it would reduce the unfair advantages that SimBoost can gain by keeping only the denser submatrix of the interaction matrix.

For Metz and Davis dataset, as SimBoost cannot handle cold drug/target problem, we had to ensure that in creating Cross-Validation folds, each drug or target appear in at least 2 folds, thus those drugs/targets with no more than 1 observation are discarded.

We also used the ToxCast dataset (U.S. EPA, 2018), containing a much larger variety of proteins (U.S. EPA, 2016). The prepared dataset contains observations for 530605 drug-target pairs. Its big size and heterogeneous proteins could help test the robustness and scalability of computational models for DTI



prediction. The ToxCast dataset contains toxicology data obtained from high-throughput *in vitro* screening of chemicals. It is curated by many different companies, under different experimental settings and with different measurements. We manually divided those endpoints into 61 different measurements for interaction strength, such that observations in each measurement are homogeneous. For ToxCast dataset, we constructed multi-task networks, in which each measurement corresponds to a neuron in the output layer. The number of observations in each measurement range from ~290 to ~160,000. As KronRLS and SimBoost are both single-task models, if we want to evaluate the performance of those two models on the ToxCast dataset, we must train 61 models for each of them, which would be an extraordinarily tedious job, so we did not run the SimBoost and KronRLS models on ToxCast. As it does not have the bottlenecks imposed by KronRLS and SimBoost, we did not filter it.

Please refer to table 1 for the sizes of the datasets after filtering.

Table 1 Dataset sizes

Dataset	Number of Drugs (compounds)	Number of target proteins	Total number of drug-target pairs used
Davis	72	442	31824
Metz	1423	170	35259
KIBA	3807	408	160296
ToxCast (no filtering)	7657	335	530605

We applied the same numerical transformation as (He et al., 2017) to the datasets. For the ToxCast dataset, we changed the inactive value from 1,000,000 to 1,000, so that there would be no large gaps in the distribution after transforming the data using the formula:  $\text{transformed} = 4 - \log_{10}(\text{original})$ .

We used the propy python package (Cao et al., 2013) to generate PSC descriptors, and manually added an entry indicating phosphorylation. The model was constructed based on the implementation of the Deepchem python package, in which RDKit (Landrum, 2014) was used; the networks were constructed using TensorFlow 1.3. In the practical application, PADME takes SMILES representations of the candidate drug as part of the input, which are transformed into graphical representations or ECFP by the program. PSC was obtained independently from this process, we saved the PSC in a standalone file and the program read it into the memory.

The experiments were conducted on a Linux server with 8 Nvidia Geforce GTX 1080Ti graphics cards, among which we could use around 4. The server has 40 logical CPU cores and 256 GB of RAM. A computer with less than 110 GB RAM might not be able to perform cross-validation for the ToxCast dataset using GraphConv-based PADME.

### 3. Experimental Design

We performed 5-fold cross validation (CV), for which every compound or target must be present in at least 2 folds for SimBoost to work. There are no such restrictions for KronRLS, since it works for cold-start data.

As cold-start prediction is an important objective in DTI prediction, we also included cold-splitting in constructing the cross-validation folds, such that all compounds in the test fold are absent from the training fold (cold-drug split), or all targets in the test fold are absent from the training fold (cold-target split). The third splitting method is called “warm split” in this paper, in which we made sure that every drug or target would appear in at least 2 folds, such that there would be no cold-start problem, otherwise SimBoost would fail. As we don’t run SimBoost and KronRLS models on ToxCast data, there is no need for us to perform warm-split on it, we then used random split in that case (if we force a warm split on ToxCast dataset, a filter threshold of 1 must be used to reduce the size of the dataset). Though (Pahikkala et al., 2014) suggested another splitting scheme which results in both cold-drug and cold-target in each validation fold, as it greatly decreases the size of the training set in each fold (4/9 of the original data instead of 4/5 in other splitting schemes), we decided that it would result in unfair comparison and did not use it in this paper.

For every dataset, we performed three types of cross-validation splitting (warm, cold-target, cold-drug), and for every CV scheme, we calculated the prediction errors of the applicable models (KronRLS and PADME for all, while SimBoost only for warm splits). To reduce the random fluctuations, we did several different splits for each splitting scheme of Davis, Metz and KIBA datasets and calculated their average values. For Davis and Metz dataset, we did 3 splits for each splitting scheme; for KIBA dataset, we did 2 for each, as it is a much bigger dataset; for ToxCast, the largest dataset, we only did 1 split for each scheme.

Not only do we have multiple splitting methods, we also use multiple different model settings and evaluation metrics. Two different PADME models (ECFP and GraphConv) are implemented to compare against each other. For every PADME model, a single-task network was trained for every splitting scheme of every dataset, except ToxCast, for which we constructed a multi-task network with 61 output neurons to avoid the excessive amount of work associated with 61 single-task networks.

For all the prediction results on the test sets, RMSE (Root Mean Squared Error), CI (Concordance Index) and R-square values are reported. Using CI as a metric in cheminformatics setting was proposed by (Pahikkala et al., 2014). It measures the probability of correctly ordering the non-equal pairs in the dataset, ranging across [0, 1], with bigger values indicating better results.

To reduce the complexity of the reported results, for ToxCast dataset, the results are averaged across the 61 different measurements, weighted by their number of observations, so the results reported for ToxCast dataset looks the same as other datasets with single endpoints.

To efficiently get the optimal values of hyperparameters (like dropout rates, batch size, learning rate, number of layers, etc.), we used Bayesian Optimization (Shahriari et al., 2016) implemented by the Python package pygpgo. We also used early stopping to determine the optimal number of training epochs needed. To guide the early stopping, we used mean(RMSE)-mean(CI) calculated on the validation set as the composite score, with the objective to minimize it. The training and validation sets used for hyperparameter searching are split randomly from the original dataset without any concern for warm or cold drug/target splits. We only store one set of hyperparameters per (dataset, model) pair that yield the best results, which were then used for all cross-validation settings for that (dataset, PADME model) pair. Note that for simplicity and to examine the robustness of PADME models, the set of hyperparameters found in the random splitting was used in all CV settings, including those with cold-drug split and cold-target split, though we believe better CV results can be achieved if the hyperparameter searching

processes are specifically designed for that CV fold split scheme, e.g., for cold-target CV folds, we could use the hyperparameters found by splitting the training and validation sets in the cold-target way.

The networks we constructed for cross-validation are rather ordinary. There are typically 2 or 3 fully-connected layers connecting the CIV to the output unit, each with thousands of neurons. Each fully-connected layer is batch-normalized.

#### 4. Experimental Results

As shown in the graphs below, we found that the ToxCast data is extremely concentrated at the non-interacting value, which led us to ignore the R-square values for this dataset. Because R-square is sensitive to the overall departure of the predicted values from the true values, we argue that the huge concentration of values has rendered R-square uninformative in measuring the performance of the model on ToxCast dataset. This concentration of values also makes RMSE less informative than it otherwise would be, so we argue that CI is the most useful metric in ToxCast prediction evaluation.

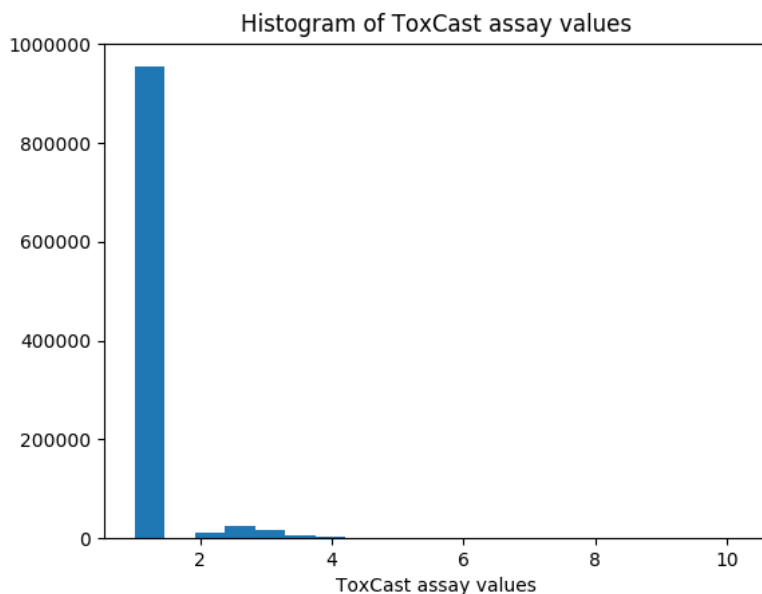


Figure 2 The histogram showing the distribution of the ToxCast assay values. The majority (over 94%) are concentrated at one inactive value.

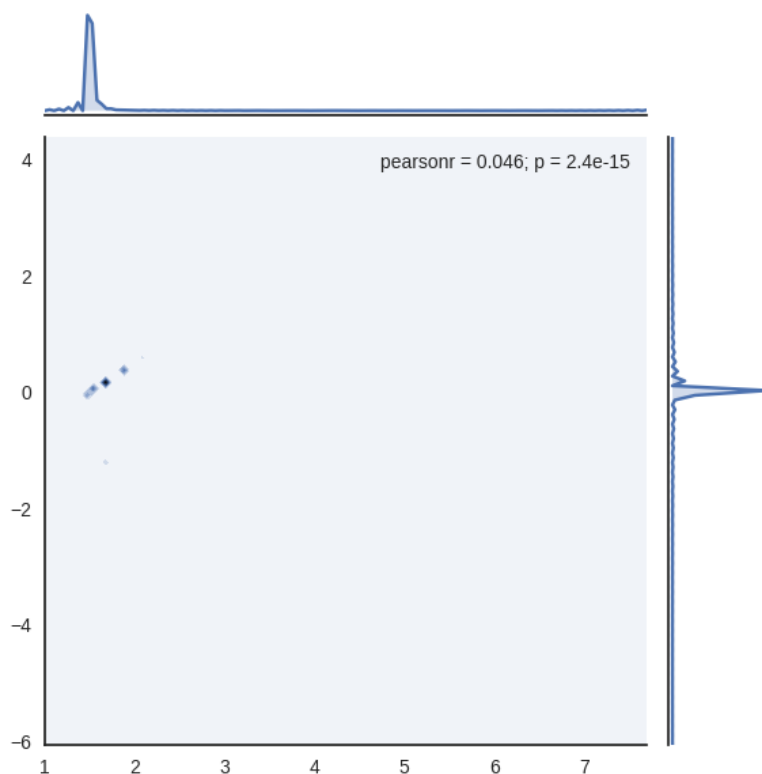


Figure 3 The contour plot of ToxCast binding subset, with the x-axis denoting the predicted value, the y-axis denoting the residual value. The frequency of x and y values are also plotted on the edges.

Tables 2~4 show the results. The bold numbers indicate the best values attained for each setting. We can see that the two versions of PADME dominate the other methods, with the only exception of SimBoost outperforming PADME-GraphConv on Metz dataset. We think it could be due to the small dataset size: PADME-GraphConv could be underfitting for Metz data, while SimBoost uses gradient boosting trees, a machine learning model better suited at small dataset than Deep Neural Networks. Because it does not use MGC, PADME-ECFP has a much smaller network than PADME-GraphConv, so the former does not suffer from underfitting as seriously on Metz dataset. However, we do not observe the same phenomenon on Davis dataset, which has a similar size and even less entities.

It is somewhat surprising that PADME-ECFP is not outperformed by PADME-GraphConv; instead, it slightly outperforms PADME-GraphConv in many cases, though in general their performances are almost indistinguishable from each other. PADME-ECFP only takes about 23% of the time and 45% the space of PADME-GraphConv in the training process and yields similar (and sometimes better) results, so PADME-ECFP is a more reasonable choice. Nonetheless, we cannot be certain that PADME-GraphConv and PADME-ECFP truly have similar performance, as there might be a better set of hyperparameters for each model that would differentiate their performances significantly. Though our results demonstrate the power of ECFP, future researchers should continue investigating MGC.

Table 2 The results measured in RMSE

		RMSE			
Dataset	Cross Validation Splitting Type	PADME-ECFP	PADME-GraphConv	SimBoost	KronRLS
Davis	Warm	<b>0.432191</b>	<b>0.432245</b>	0.481973	0.572941
	Cold Drug	<b>0.785358</b>	0.806446	NA	0.840484
	Cold Target	<b>0.560054</b>	0.578407	NA	0.659645
Metz	Warm	<b>0.552927</b>	0.59926	0.581254	0.781284
	Cold Drug	<b>0.711698</b>	0.742916	NA	0.784291
	Cold Target	<b>0.791535</b>	0.818935	NA	0.898888
Kiba	Warm	0.432138	<b>0.418691</b>	0.468883	0.656647
	Cold Drug	<b>0.602012</b>	0.620291	NA	0.702427
	Cold Target	<b>0.616767</b>	0.623449	NA	0.681109
ToxCast	Warm (Random)	<b>0.405633</b>	0.407789	NA	NA
	Cold Drug	<b>0.444847</b>	<b>0.445019</b>	NA	NA
	Cold Target	<b>0.486978</b>	0.494392	NA	NA

Table 3 The results across the datasets measured in Concordance Index.

		Concordance Index			
Dataset	Cross Validation Splitting Type	PADME-ECFP	PADME-GraphConv	SimBoost	KronRLS
Davis	Warm	<b>0.903882</b>	<b>0.903892</b>	0.887096	0.87578
	Cold Drug	0.716298	<b>0.720008</b>	NA	0.692436
	Cold Target	<b>0.855025</b>	0.844831	NA	0.80751
Metz	Warm	<b>0.807563</b>	0.794003	0.794381	0.748522
	Cold Drug	<b>0.742403</b>	0.741041	NA	0.709156
	Cold Target	0.698305	<b>0.707959</b>	NA	0.647
Kiba	Warm	0.857452	<b>0.863699</b>	0.840456	0.783103
	Cold Drug	<b>0.773099</b>	0.754999	NA	0.688972
	Cold Target	<b>0.771671</b>	0.767902	NA	0.7122
ToxCast	Warm (Random)	0.796547	<b>0.798712</b>	NA	NA
	Cold Drug	0.720573	<b>0.72858</b>	NA	NA
	Cold Target	0.684814	<b>0.690501</b>	NA	NA

Table 4 The results across the datasets, measured in R square.

		R-square			
Dataset	Cross Validation Splitting Type	PADME-ECFP	PADME-GraphConv	SimBoost	KronRLS
Davis	Warm	0.760728	<b>0.76099</b>	0.703138	0.580148
	Cold Drug	<b>0.191118</b>	0.115659	NA	0.047802
	Cold Target	<b>0.594517</b>	0.569119	NA	0.439302
Metz	Warm	<b>0.667115</b>	0.608763	0.632297	0.335489

	Cold Drug	<b>0.446423</b>	0.395589	NA	0.328515
	Cold Target	<b>0.31438</b>	0.267742	NA	0.11295
Kiba	Warm	0.745663	<b>0.761212</b>	0.700674	0.412822
	Cold Drug	<b>0.5058</b>	0.472761	NA	0.326592
	Cold Target	<b>0.479066</b>	0.467213	NA	0.363054
ToxCast	Warm (Random)	NA	NA	NA	NA
	Cold Drug	NA	NA	NA	NA
	Cold Target	NA	NA	NA	NA

From the tables we can observe an interesting phenomenon: when there are many compounds and few targets in the training set, the cold-drug predictions tend to outperform the cold-target predictions; on the other hand, when there are many targets and few compounds, the cold-target predictions tend to be better than the cold-drug ones. We hypothesize that it is because the models can be more robust in entities (drugs or targets) with more information in the training set, thus performing better in the corresponding scenario. This trend is not only present in PADME models, but in KronRLS as well. It seems that the models also require much more types of compounds than proteins for learning their chemical features, as can be seen from the KIBA dataset, whose cold-drug and cold-target performances are very similar, though it has 3807 compounds and only 408 proteins. And, as expected, there is a universal trend that the performance of warm splits is always better than that of cold-drug or cold-target splits.

The fact that PADME outperforms both SimBoost and KronRLS demonstrates the power of deep neural networks to learn complicated nonlinear relationships between drug-target pairs and interaction strength. Furthermore, the results presented might be an understatement of the real performance of PADME models in cold-drug and cold-target scenarios, as the training and validation sets for hyperparameter searching are randomly split, resulting in a set of hyperparameters that suit well for randomly split CV folds, but perhaps not for cold-drug and cold-target folds. This deliberate unfair comparison testifies the robustness of PADME models.

## Case Studies

After the previous experiments are done, we decided to do some special experiments to further validate the predictions of PADME.

Androgen receptor (AR) is an important target protein in Prostate Cancer (Yap et al., 2016), which the authors are most familiar with. So our case studies are mainly focused on AR.

We used all compounds in NCI60 data, but only AR as the target protein. For prediction, we used both PADME models trained on ToxCast random-split CV folds, and took the average of the predictions made by PADME-ECFP and PADME-GraphConv. The reason we chose ToxCast is that it has the most diverse set of compounds and proteins. Because there are 61 outputs in PADME models trained on ToxCast data, we had to propose a set of coefficients to calculate a composite AR antagonist score (details in the supplementary material), for which we expect the compounds with higher scores would show stronger activity in NCI60 dataset. We then ordered the averaged AR antagonist scores in a descending

order. We only consider the logGI50 values in NCI60 dataset, which is also real-valued. The smaller the logGI50 value, the more active the compound.

We did 2 different analyses: set-based analysis and list-based analysis.

### 1. Set-based analysis

We used only the Prostate Cancer panel in the NCI60 dataset, in which there were 5 cell lines, but 3 of the cell lines had very few observations, so we only chose PC-3 and DU-145, both of which has more than 35,000 observations.

We report the results separately for each cell line. For each of them, we took the top 100, top 1000, top 15000 and all compounds that appear in averaged AR antagonist score. We skipped those compounds in predicted AR antagonist score list that were absent from the cell line to ensure that the top-n set contains n compounds. Say we have a top-100 list for DU-145, the 100<sup>th</sup> compound in the list is actually not in the top 100 in the sorted AR antagonist score list, because there are compounds in AR score list that do not have observations for DU-145.

We calculated the mean and standard deviation of the logGI50 values for those top-n compounds. Because we don't consider the order among the top-n compounds, we call it set-based analysis. Table 5 presents the values for the two prostate cancer cell lines.

*Table 5 table for set-based results, mean and standard deviation of logGI50 values in top-n compounds for AR interaction.*

Panel	top_n	cell line	mean value	standard deviation
Prostate	35159	DU-145	-4.64514	0.91656
Prostate	15000	DU-145	-4.87862	1.013378
Prostate	1000	DU-145	-5.56875	1.528878
Prostate	100	DU-145	-7.16448	1.401604
Prostate	35238	PC-3	-4.71778	0.92443
Prostate	15000	PC-3	-4.96484	0.993843
Prostate	1000	PC-3	-5.55062	1.436045
Prostate	100	PC-3	-6.99828	1.466907

Based on the values in table 5, we conduct a series of one sample t-tests. For example, in Table 6, the entry corresponding to (100, 1000) is obtained by performing a t-test on top 100 compounds against the top 1000 compounds, in which H0 is: the mean logGI50 values of the hypothetical group that the top 100 compounds in AR score in DU-145 dataset belong to, equals the mean of that of top 1000 compounds (-5.56875). In other words, the top 100 compounds are obtained from the top 1000 by pure chance. H1 is: the mean logGI50 values of the hypothetical group that the top 100 compounds in AR score belong to, is smaller than the mean of that of top 1000 compounds (-5.56875). In other words, the top 100 compounds in AR scores are truly more active than the top 1000 compounds. Table 7 is the same operations on PC-3 dataset.

We can see that the null hypotheses are all strongly rejected, which shows a consistent trend that the compounds with a high predicted AR score tend to be more active in the prostate cancer cell lines.

Table 6 base top-k comparing against other top-k's for DU-145. A one sample t-test is conducted for each filled entry, where H0 is that both top-k's have identical means, while H1 is that the base top-k has a smaller mean.

Cell line: DU-145	Top-k to compare against		
Base top-k	1000	15000	All (35159)
15000	-	-	t-score: -28.2176; p value: 1.95E-49
1000	-	t-score: -14.2744; p value: 4.53E-26	t-score: -19.1036; p value: 2.80E-35
100	t-score: -11.385; p value: 5.37E-20	t-score: -16.3089; p value: 4.18E-30	t-score: -17.9747; p value: 3.06E-33

Table 7 base top-k comparing against other top-k's for PC-3. Calculated in the same way as the previous table.

Cell line: DU-145	Top-k to compare against		
Base top-k	1000	15000	All (35159)
15000	-	-	t-score: -30.4452; p value: 2.28E-52
1000	-	t-score: -12.8994; p value: 3.18E-23	t-score: -18.3397; p value: 6.58E-34
100	t-score: -9.869; p value: 1.06E-16	t-score: -13.8621; p value: 3.16E-25	t-score: -15.5463; p value: 1.28E-28

## 2. List-based analysis

Similar to the set-based analysis, we also used Prostate Cancer panel with PC-3 and DU-145 cell lines. We also skipped those absent compounds to ensure the top-n list has n compounds. Unlike the previous analysis, we used Normalized Discounted Cumulative Gain (NDCG), a metric often used in data mining to examine the quality of ranking (Jarvelin and Kekalainen, 2002), in which we used the classical logarithmic discount, and used logGI50 as the relevance score of the compound. NDCG values have the range [0, 1], the higher the value is, the better the ranking quality. We call it list-based analysis because the order among the top-n compounds could influence the NDCG values. Please refer to table 8 for results.

Table 8 The table for NDCG of the ranked list (ranked by AR score) of compounds in prostate cancer cell lines.

Panel	top_n	cell line	nDCG
Prostate	35159	DU-145	0.908682
Prostate	15000	DU-145	0.862253
Prostate	1000	DU-145	0.766965
Prostate	500	DU-145	0.789845
Prostate	100	DU-145	0.790048
Prostate	50	DU-145	0.761455
Prostate	10	DU-145	0.713888
Prostate	35238	PC-3	0.917356
Prostate	15000	PC-3	0.871041
Prostate	1000	PC-3	0.763712
Prostate	500	PC-3	0.779395



Prostate	100	PC-3	0.777934
Prostate	50	PC-3	0.75385
Prostate	10	PC-3	0.694859

It could be surprising that the more compounds are taken into consideration, the higher the NDCG value becomes, since we expect those top compounds should show stronger signal of being potent and thus be ordered more correctly, while those weaker compounds are more blurred and should be ordered more incorrectly. The truth is that NDCG value tends to approach 1 as the number of items in the list increases (Wang et al., 2013). In general, the NDCG values are fairly high across all top-n values, and that for the top-100 are larger than top-1000, which shows a better ranking quality for top compounds.

To summarize, we believe the case studies showed that the predictions of PADME agree with experimental results in NCI60.

## Discussion

PADME is a very general and versatile framework, compatible with a large variety of different protein and compound featurization methods. By combining different protein descriptors like PSSM and other molecule featurization schemes like Weave (Kearnes et al., 2016), many variants of PADME can be constructed, whose performance can be compared against each other. In fact, we used the Weave implementation in DeepChem as a molecular featurization method and ran hyperparameter searching on it, but the result was not as good as ECFP or GraphConv, and it consumed much more time and memory than the other two, so we did not pursue it any further.

It is also possible to use CNN or RNN to learn a latent feature vector to represent the proteins, based on its amino acid sequence information, instead of using fixed-rule protein descriptors like PSC as the input, so that the whole model can be trained in a completely end-to-end fashion without standalone components of the network like PSC in our implementation, making the network structure more “symmetrical”. Actually, it was already attempted by (Ozturk et al., 2018), who showed a performance similar to PADME, but they did not use cross-validation to get average performances, they only ran different models on the same test set, which was just 1/6 the size of the whole dataset, so we think there is still much room for improvement in that direction.

We only used simple FNN in our model from the Combined Input Vector to the output, but other types of Neural Networks might be able to generate better results, like Highway Networks (Srivastava et al., 2015), which allows the units in the network to take shortcuts, circumventing the huge amounts of layers in some networks.

Pretraining also has the potential to improve our model, but we did not include it, because it might be difficult for the community to compare the real performance of PADME with other models.

## Conclusion

To tackle DTI prediction problem from a new angle, we devised PADME framework that utilizes deep neural networks for this task. PADME incorporates both compound and target protein information, so it can handle the cold-start problem, which most current deep-learning based models for DTI prediction cannot do. Predicting real-valued endpoints also makes it desirable for problems requiring finer

granularity than the simple binary classification. We are the first to incorporate MGC with protein descriptors in the DTI task, and have shown PADME consistently outperforming state-of-the-art methods, but surprisingly enough, PADME based on MGC (more specifically, GraphConv) does not outperform PADME based on ECFP. PADME is also much more scalable than the state-of-the-art models for DTI regression task, namely SimBoost and KronRLS. Another contribution of ours is the use of ToxCast dataset in DTI prediction problems, we believe future researches should run their models on this dataset in addition to the other datasets, including Davis, Metz and KIBA.

We also predicted the interaction strength between compounds and androgen receptor (AR), the compounds predicted to have strong interactions with AR indeed showed higher level of activities in NCI60 dataset prostate cancer cell lines, suggesting that PADME has the potential to be applied in drug development.

With the great compatibility of PADME to different drug molecule and target protein featurization methods, we believe that future researches could propose more PADME variants that advance the frontier of DTI prediction researches.

## Acknowledgements

The authors would like to thank the help and suggestions received from our fellow lab members, including but not limited to Zaccary Alperstein, Michael Lllamosa, Fuqiang Ban, Hossein Sharifi, Jiayi Tang, Beidou Wang, Sahand Khakabimamaghani and Michael Hsing. We also express our gratitude towards our family and friends, especially Wen Xie, Yue Zhang, Aster Li, Lan Lin, Xuyan Qian, Si Chen, Fengjie Lun and Stephen Tseng; and, most important of all, the late Mr. Xiefu Zang.

## References:

Cao D. S., Xu Q. S., and Liang Y. Z. (2013). Propy: a tool to generate various modes of Chou's PseAAC. *Bioinformatics* 2013, 29 (7), 960–962.

Dahl G. E., Jaitly N., Salakhutdinov R. (2014). Multi-task neural networks for QSAR predictions[J]. *Computer Science*, 2014, arXiv: 1406.1231.

Davis M. I., Hunt J. P., Herrgard S., Ciceri P., Wodicka L. M., Pallares G., Hocker M., Treiber D. K., Zarrinkar P. P. (2011) Comprehensive analysis of kinase inhibitor selectivity. *Nature Biotechnology*. 29(11):1046–1051

Ding H., Takigawa I., Mamitsuka H., Zhu S. (2014) Similarity-based machine learning methods for predicting drug–target interactions: a brief review. *Briefings in Bioinformatics* 15(5):734–747

Duvenaud D., Maclaurin D., Iparraguirre J., Bombarell R., Hirzel T., Guzik A., and Adams R. (2015). Convolutional networks on graphs for learning molecular fingerprints. In *Advances in Neural Information Processing Systems*, pages 2215–2223, 2015.

Gomes J., Ramsundar B., Feinberg E. N., and Pande V. S. (2017). Atomic Convolutional Networks for Predicting Protein-Ligand Binding Affinity. arXiv:1703.10603v1

Goodfellow I., Bengio Y. and Courville A. (2016). Deep Learning. MIT Press. Available at: <http://www.deeplearningbook.org>.

He T., Heidemeyer M., Ban F. et al. (2017). SimBoost: a read-across approach for predicting drug–target binding affinities using gradient boosting machines. *Journal of Cheminformatics* (2017) 9:24 DOI 10.1186/s13321-017-0209-z

Jarvelin K. and Kekalainen J. (2002). Cumulated gain-based evaluation of IR techniques. *ACM Transactions on Information Systems (TOIS)*, 20(4):422–446, 2002.

Kearnes S., McCloskey K., Berndl M., Pande V., Riley P. (2016). Molecular Graph Convolutions: Moving Beyond Fingerprints. arXiv:1603.00856v3

Landrum G. (2014). RDKit: Open-source cheminformatics; <http://www.rdkit.org>.

LeCun, Y., Bengio, Y., and Hinton, G. E. (2015). Deep Learning. *Nature* 521, 436–444. doi: 10.1038/nature14539

Ma J., Sheridan R. P., Liaw A., et al. (2015). Deep neural nets as a method for quantitative structure-activity relationships[J]. *Journal of Chemical Information and Modeling*, 2015, 55(2): 263-274.

Mayr A., Klambauer G., Unterthiner T., et al. (2016). DeepTox: toxicity prediction using deep learning. *Frontiers in Environmental Science*, 2016, 3(8): 80.

Metz J. T., Johnson E. F., Soni N. B., Merta P. J., Kife L., Hajduk P. J. (2011) Navigating the kinome. *Nature Chemical Biology*. 7(4):200–202

Mousavian Z., Khakabimamaghani S., Kavousi K., Nejad A. M. (2016). Drug-target interaction prediction from PSSM based evolutionary information. *Journal of Pharmacological and Toxicological Methods*, 78, (2016), 42-51.

Öztürk H., Ozkirimli E., Özgür A. (2018). DeepDTA: Deep Drug-Target Binding Affinity Prediction. arXiv:1801.10193v2 [stat.ML]

Pahikkala T., Airola A., Pietila S. et al. (2014). Toward more realistic drug-target interaction predictions. *Briefings in Bioinformatics* 16(2):325–337. doi:10.1093/bib/bbu010

Qiu T, Qiu J, Feng J, Wu D, Yang Y, Tang K, Cao Z, Zhu R (2016) The recent progress in proteochemometric modelling: focusing on target descriptors, cross-term descriptors and application scope. *Briefings in bioinformatics*. doi: 10.1093/bib/bbw004

Ramsundar B., Kearnes S., Riley P., Webster D., Konerding D., Pande V. (2015). Massively Multitask Networks for Drug Discovery. arXiv:1502.02072 [stat.ML]

Rogers D. and Hahn M. (2010) Extended-connectivity fingerprints. *Journal of Chemical Information and Modeling*. 2010, 50(5), 742–754

Schmidhuber J. (2015). Deep learning in neural networks: an overview. *Neural Networks*. 61, 85–117. doi: 10.1016/j.neunet.2014.09.003

Shahriari, B., Swersky, K., Wang, Z., Adams, R. P., Freitas N. D. (2016) Taking the human out of the loop: a review of Bayesian Optimization. *Proceedings of the IEEE*. Vol. 104, No. 1, January 2016.

Sharma, A., et al. (2013). A feature extraction technique using bi-gram probabilities of position specific scoring matrix for protein fold recognition. *Journal of Theoretical Biology*, 320, 41-46.

Shoemaker R. H. (2006). The NCI60 human tumour cell line anticancer drug screen. *Nature Reviews Cancer* 6, 813–823.

Srivastava R. K., Greff K., Schmidhuber J. (2015). Highway Networks. arXiv:1505.00387v2 [cs.LG]

Tang J, Szwajda A, Shakyawar S, Xu T, Hintsanen P, Wennerberg K, Aittokallio T. (2014). Making sense of large-scale kinase inhibitor bioactivity data sets: a comparative and integrative analysis. *Journal of Chemical Information and Modeling*. 54(3):735–743

Tran H. A., Ramsundar B., Pappu A. S., Pande V. (2017). Low Data Drug Discovery with One-Shot Learning. *ACS Central Science*, 2017, 3, 283-293

Unterthiner T., Mayr A., Klambauer G. et al. (2014). Multi-Task Deep Networks for Drug Target Prediction. *Neural Information Processing System*, 2014: 1-4.

Wallach I., Dzamba M., and Heifets A. (2015). AtomNet: A Deep Convolutional Neural Network for Bioactivity Prediction in Structure-based Drug Discovery. *Mathematische Zeitschrift*, 2015, arXiv: 1510.02855.

Yining Wang, Liwei Wang, Yuanzhi Li, Di He, Wei Chen, Tie-Yan Liu. (2013). A Theoretical Analysis of Normalized Discounted Cumulative Gain (NDCG) Ranking Measures. In *Proceedings of the 26th Annual Conference on Learning Theory (COLT 2013)*.

Wen M., Zhang Z., Niu S., Sha H. et al. (2017). Deep-Learning-Based Drug–Target Interaction Prediction. *Journal of Proteome Research*, 2017, 16, 1401-1409. DOI: 10.1021/acs.jproteome.6b00618

Westen GJ, Wegner J, Ijzerman AP, van Vlijmen HW, Bender A (2011) Proteochemometric modeling as a tool to design selective compounds and for extrapolating to novel targets. *Medicinal Chemistry Communications*. 2: 16–30.

Wu, Z., Ramsundar, B., Feinberg, E. N., Gomes, J., Geniesse, C., Pappu, A. S., Leswing, K. and Pande V. (2017). MoleculeNet: A Benchmark for Molecular Machine Learning. arXiv:1703.00564 [cs.LG]

Xiao, N., Xu, Q., & Cao, D. (2013). Protr: Protein Sequence Feature Extraction with R. R package version 0.2-0.

Xu Y. and Pei J. (2017). Deep Learning for Chemoinformatics. *大数据*, Volume 3, number 2. DOI: 10.11959/j.issn.2096-0271.2017019 [in Chinese]

U.S. EPA. 2018. ToxCast Summary Files from invitrodb\_v2. Retrieved from <https://www.epa.gov/chemical-research/toxicity-forecaster-toxcasttm-data> on March 22, 2018. Data released October 2015.

## Supplementary Materials

### Datasets preparation

#### Davis dataset

Compound names were extracted from Davis dataset.<sup>1,2</sup> The corresponding compound CIDs and SMILES strings were extracted from PubChem.<sup>3</sup> NCBI GenBank Protein accession numbers from Davis dataset were used to download the corresponding amino acid sequences via NCBI Batch Entrez.<sup>4</sup> As sequences with accession numbers P0C1S8 and P0C264 were no longer available in GenBank Protein, their updated versions P0C1S8.2 and P0C264.2 were downloaded. Protein sequences were modified according to descriptions from the original paper, e.g. mutations were introduced and only sequences corresponding to specified domains, if any, were left (domains were detected according to GenBank Protein domains annotation).

#### Metz dataset

Kinase names extracted from Metz Dataset<sup>5,6</sup> were searched in KinBase.<sup>7</sup> Found gene names were saved and the corresponding amino acid sequences were extracted from Human Kinome Database (downloaded from KinBase – The Kinase Database<sup>8,9</sup> and containing 538 human kinases). There were compounds with different ChEMBL IDs but have the same smiles strings, with different activity measurement results, so we neglected them in the execution of the program.

#### KIBA dataset

ChEMBL IDs and protein IDs were extracted from KIBA dataset.<sup>10,11</sup> Canonical smiles strings were loaded from ChEMBL database<sup>12,13</sup> via ChEMBL webresource client.<sup>14,15</sup> NCBI GenBank Protein accession numbers from KIBA dataset were used to download corresponding sequences via NCBI Batch Entrez.<sup>4</sup>

#### ToxCast Dataset

The following file archives were downloaded from ToxCast website:

- 1) INVITRODB\_V2\_SUMMARY (October 2015)<sup>16</sup>. File Assay\_Summary\_151020.xls contains summary information about assays. File oldstyle\_ac50\_Matrix\_151020.xls contains summary of testing results.
- 2) DSSTox\_ToxCastRelease\_20151019.<sup>17</sup> File DSSTox\_ToxCastRelease\_20151019.xls contains summary of chemicals tested.

Compound structures contained in DSSTox\_ToxCastRelease\_20151019.xls were processed using MOE 2013.8<sup>18</sup> as follows: water samples, mixtures with unidentified content, and polymers were excluded. Structures were “washed” by means of MOE: salts were split and the largest part of each salt was retained, the structures were then neutralized. Compounds containing atoms other than C, N, S, O, F, Cl, Br, I, P, B, Si, H were removed. Duplicated structures were filtered using MOE sdsort<sup>19</sup> tool.

Only assays with single corresponding intended target in the file Assay\_Summary\_151020.xls were selected and split in groups. For them Uniprot IDs were extracted and used to download protein sequences from Uniprot.<sup>20,21</sup>

## References

- 1 Davis, M. I. *et al.* Comprehensive analysis of kinase inhibitor selectivity. *Nat Biotechnol* **29**, 1046-1051, doi:10.1038/nbt.1990 (2011).
- 2 *Davis Dataset (Supplementary Tables 3 and 4)*, <<https://www.nature.com/articles/nbt.1990#supplementary-information>>.
- 3 *PubChem website*, <<https://pubchem.ncbi.nlm.nih.gov/>>.
- 4 *NCBI Batch Entrez*, <<https://www.ncbi.nlm.nih.gov/sites/batchentrez>>.
- 5 Metz, J. T. *et al.* Navigating the kinome. *Nat Chem Biol* **7**, 200-202, doi:10.1038/nchembio.530 (2011).
- 6 *Metz Dataset (Supplementary Table 2)*, <<https://www.nature.com/articles/nchembio.530#supplementary-information>>.
- 7 *KinBase. The Kinase Database website*, <<http://kinase.com/web/current/kinbase/>>.
- 8 *KinBase. The Kinase Database. Human Kinome Database website*, <<http://kinase.com/web/current/kinbase/genes/SpeciesID/9606/>>.
- 9 Manning, G., Whyte, D. B., Martinez, R., Hunter, T. & Sudarsanam, S. The protein kinase complement of the human genome. *Science* **298**, 1912-1934, doi:10.1126/science.1075762 (2002).
- 10 Tang, J. *et al.* Making sense of large-scale kinase inhibitor bioactivity data sets: a comparative and integrative analysis. *J Chem Inf Model* **54**, 735-743, doi:10.1021/ci400709d (2014).
- 11 *KIBA Dataset (Supplementary File ci400709d\_si\_002.xlsx)*, <<https://pubs.acs.org/doi/suppl/10.1021/ci400709d>>.
- 12 *ChEMBL database (release chembl\_23)*, <[http://ftp.ebi.ac.uk/pub/databases/chembl/ChEMBLdb/releases/chembl\\_23/](http://ftp.ebi.ac.uk/pub/databases/chembl/ChEMBLdb/releases/chembl_23/)>.
- 13 Gaulton, A. *et al.* The ChEMBL database in 2017. *Nucleic Acids Res* **45**, D945-D954, doi:10.1093/nar/gkw1074 (2017).

- 14 *ChEMBL webresource client* <[https://github.com/chembl/chembl\\_webresource\\_client](https://github.com/chembl/chembl_webresource_client)>.
- 15 Davies, M. *et al.* ChEMBL web services: streamlining access to drug discovery data and utilities. *Nucleic Acids Res* **43**, W612-620, doi:10.1093/nar/gkv352 (2015).
- 16 U.S. EPA. 2018. ToxCast and Tox21 Summary Files invitrodb\_v2. Retrieved from <https://www.epa.gov/chemical-research/toxicity-forecaster-toxcasttm-data> on March 22, 2018. Data released October 2015.
- 17 U.S. EPA. 2018. ToxCast & Tox21 Chemicals Distributed Structure-Searchable Toxicity Database DSSTox\_20151019. Retrieved from <https://www.epa.gov/chemical-research/toxicity-forecaster-toxcasttm-data> on March 22, 2018. Data release October 2015.
- 18 Molecular Operating Environment (MOE), 2013.08; Chemical Computing Group ULC, 1010 Sherbooke St. West, Suite #910, Montreal, QC, Canada, H3A 2R7, 2018.
- 19 sdsort.
- 20 *UniprotKB website*, <<https://www.uniprot.org/uniprot/>>.
- 21 The UniProt, C. UniProt: the universal protein knowledgebase. *Nucleic Acids Res* **45**, D158-D169, doi:10.1093/nar/gkw1099 (2017).